

Universal intensity statistics of multifractal resonance states

Konstantin Clauß,¹ Felix Kunzmann,¹ Arnd Bäcker,^{1,2} and Roland Ketzmerick^{1,2}

¹*Technische Universität Dresden, Institut für Theoretische Physik and Center for Dynamics, 01062 Dresden, Germany*

²*Max-Planck-Institut für Physik komplexer Systeme, Nöthnitzer Straße 38, 01187 Dresden, Germany*

(Dated: April 26, 2021)

We conjecture that in chaotic quantum systems with escape the intensity statistics for resonance states universally follows an exponential distribution. This requires a scaling by the multifractal mean intensity which depends on the system and the decay rate of the resonance state. We numerically support the conjecture by studying the phase-space Husimi function and the position representation of resonance states of the chaotic standard map, the baker map, and a random matrix model, each with partial escape.

I. INTRODUCTION

A detailed understanding of the structure and fluctuations of eigenstates is essential for the description of complex systems. For closed systems with classically ergodic dynamics almost all quantum eigenstates converge weakly towards the uniform measure on phase space as proven by the quantum ergodicity theorem [1–5]. This uniform limit is also established for quantum maps [6, 7]. More detailed information is provided by the statistical fluctuations of eigenstates. For quantum billiards the random wave model [8] implies a Gaussian distribution of the eigenstate amplitudes, leading to a universal exponential distribution of the intensities, as confirmed, e.g., in Refs. [9–12]. For quantum maps with fully chaotic classical dynamics the eigenvector statistics is expected to be described by those of random matrices, originally introduced to describe the statistics of transition strengths of complex nuclei [13, 14]. For systems without symmetry this leads to an exponential distribution of the intensities, as demonstrated, e.g., in Refs. [15–19]. Restricted random wave models have been proposed to describe for example systems with a mixed phase space [20, 21] and other non-isotropic cases [22–24]. The statistical properties of eigenstates play an important role in the context of many-body systems, see Refs. [25–27] and references therein.

In general, physical systems are not completely closed. They often show (partial) loss of particles or intensity in some interaction region [28], e.g., as in the three-disk scattering system [29–31] or in optical microcavities [32]. Such scattering systems are described by resonance poles and the corresponding resonance states ψ which have a decay rate γ . The distribution of decay rates is given by a fractal Weyl law in systems with full escape [33–41], and has been studied in systems with partial escape [42–45].

Resonance states of chaotic systems with escape are generally not uniformly distributed, e.g., see Fig. 1 (b). Instead, they show a strong dependence on the phase-space region and decay rate γ . The average structure of resonance states with decay rate γ is described by a multifractal measure on phase space [46–56]. Such measures are conditionally invariant [28, 57], i.e., invariant under the corresponding classical dynamics with escape up to a global decay with rate γ . The most recent classical construction of such measures describes the average structure of resonance states quite well, but still shows deviations in the semiclassical limit for most γ [55].

Individual resonance states of systems with escape have been discussed in terms of scarring on periodic orbits [58], for microcavities [47, 59–61] and quantum maps [62–65]. However, a systematic study of the statistical properties of individual resonance states is still missing, even in fully chaotic systems with escape. In particular, the question arises if there are universal properties of the intensity statistics.

These intensity fluctuations occur in the position representation of resonance states in chaotic scattering systems like the three-disk billiard. They also play an important role in the lasing properties of optical microcavities, which depend on individual resonance states. Knowledge of the intensity statistics might also allow to distinguish enhancement due to fluctuations from enhancement due to scarring on periodic orbits.

In this paper we conjecture that in chaotic quantum systems with escape a suitably scaled intensity statistics for resonance states universally follows an exponential distribution with mean one. To this end we scale by the mean intensity which depends on the system, the decay rate of the resonance state, and the phase-space region. We numerically support the conjecture by studying the phase-space Husimi function and the position representation of resonance states of the standard map with chaotic dynamics, the baker map, and a random matrix model, each with partial escape.

The paper is organized as follows. In Sec. II we introduce the class of quantum maps with escape and illustrate the scaled intensities for resonance states. In Sec. III we propose a conjecture about the statistics of these scaled intensities. In Sec. IV we present numerical support for the conjecture in two exemplary quantum maps with escape and for a random matrix model. The results are summarized in Sec. V.

II. SCALED INTENSITIES OF RESONANCE STATES

We consider dynamical systems which are described by a time-discrete map M on a bounded phase space Γ , originating, e.g., from time-periodically driven systems or a Poincaré section of an autonomous system. Escape (or gain) is introduced for such a system by a reflectivity function $r: \Gamma \rightarrow \mathbb{R}_{\geq 0}$, such that $r(x)$ describes the factor by which the intensity at the phase-space point x changes per time step [28]. Regions with escape (gain) are described by $r < 1$ ($r > 1$).

The corresponding quantum map with escape (or gain) is

composed of the closed systems time evolution operator \hat{U} of dimension $N = 1/h$ (quantizing the map M using an effective Planck's constant h) and some reflection operator $\hat{R} = \text{Op}_N \sqrt{r}$ (quantizing the reflectivity function r) [66]. Without loss of generality we assume that escape takes place before the closed time evolution such that the quantum map with escape is defined as

$$\hat{U}_r = \hat{U}\hat{R}. \quad (1)$$

The eigenvalue equation

$$\hat{U}_r \psi = e^{-i\theta - \gamma/2} \psi \quad (2)$$

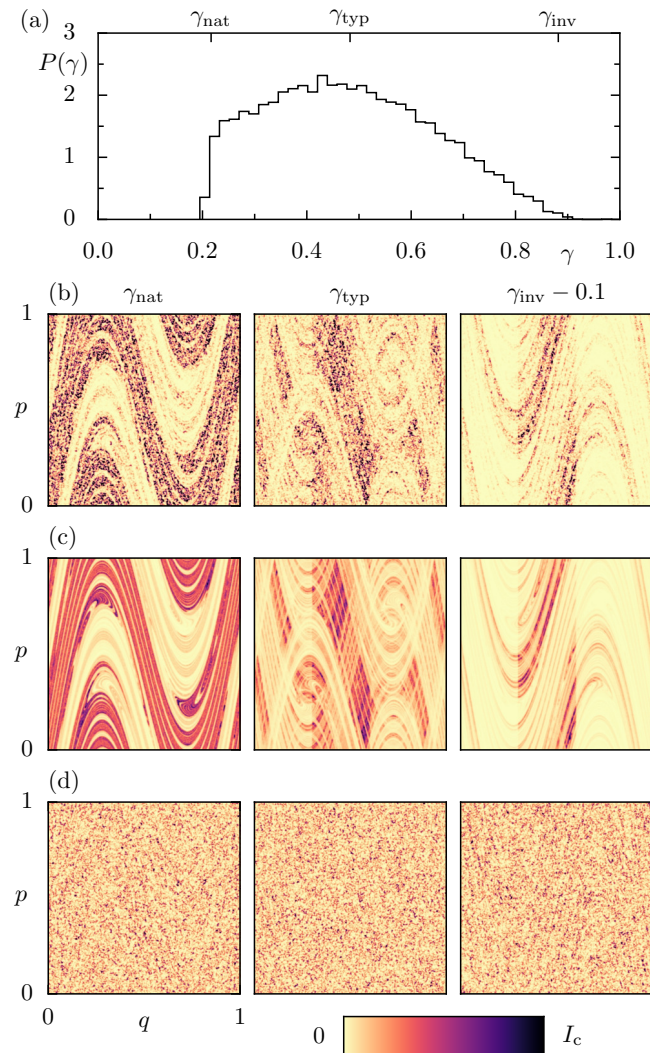


Figure 1. (a) Distribution of quantum decay rates γ for the chaotic standard map with partial escape, defined in App. A, with $h = 1/16000$. Classical decay rates $\gamma_{\text{nat}} \approx 0.22$, $\gamma_{\text{typ}} \approx 0.48$, $\gamma_{\text{inv}} \approx 0.88$ are indicated. (b) Husimi functions H_ψ for three exemplary resonance states ψ with decay rates γ_{nat} , γ_{typ} , and $\gamma_{\text{inv}} - 0.1$. (c) Averaged Husimi function $\langle H \rangle_\gamma$ of $n_{\text{avg}} = 200$ resonance states close to each γ . The same colormap with maximum I_c is used for each pair of individual and average Husimi function, where $I_c = \max_\Gamma \langle H \rangle_\gamma$. (d) Scaled Husimi functions \tilde{H}_ψ , see Eq. (4), visualized with $I_c = 8$.

defines resonance states ψ with decay rate γ , i.e., their norm decays in each application of \hat{U}_r by a factor of $e^{-\gamma}$. In autonomous scattering the phase θ is related to the energy and γ to the width of resonance poles [67, 68]. Note that due to the non-unitarity of \hat{U}_r the set of all right eigenfunctions $\{\psi_k\}_{k=1}^N$ is generally non-orthogonal, $\langle \psi_k | \psi_l \rangle \neq 0$ for $k \neq l$. Together with the eigenfunctions $\{\phi_j\}_{j=1}^N$ of the adjoint \hat{U}_r^\dagger , called left eigenfunctions, a dual basis of the Hilbert space is formed. Without loss of generality we investigate the intensity statistics of right eigenfunctions in the following. Note that the fixed reflectivity function $r(x)$ implies that in the semiclassical limit, $N \rightarrow \infty$, escape takes place from a large region compared to the Planck cell h .

As an illustrative example we choose a paradigmatic two-dimensional chaotic map, the standard map with partial escape, as defined in App. A. For this system we show numerical results in Fig. 1. The distribution of decay rates γ , see Fig. 1 (a), extends approximately from the natural to the inverse decay rate of the classical map, $\gamma_{\text{nat}} \lesssim \gamma \lesssim \gamma_{\text{inv}}$, [55] and is peaked around the so-called typical decay rate γ_{typ} of classically ergodic orbits [43].

For the intensity statistics of resonance states ψ we use as an example the Husimi function H_ψ [69], which is a smooth probability distribution on phase space. It is defined using the overlap of the state ψ with a coherent state $\alpha(x)$ centered at some phase-space point $x = (q, p)$,

$$H_\psi(x) = h^{-1} |\langle \alpha(x) | \psi \rangle|^2. \quad (3)$$

In the following numerical illustrations the width of $\alpha(x)$ is chosen to be symmetric in phase space. Figure 1 (b) shows the Husimi function for three resonance states with different decay rates γ . They fluctuate by many orders of magnitude on the scale of Planck's constant h . Their intensities clearly depend on the phase-space region and decay rate. The intensity statistics over all resonance states gives a non-universal, system specific distribution. Even at a single phase-space point one finds a non-universal distribution (not shown).

It turns out to be essential to consider the strong γ -dependence of resonance states. Their phase-space structure changes significantly with γ from an orientation along the classical unstable direction (close to γ_{nat}) to the stable direction (close to γ_{inv}) [55]. This is prominently seen in the average Husimi function $\langle H \rangle_\gamma(x)$ in Fig. 1 (c), which is defined as an average over n_{avg} Husimi functions with decay rates close to the given decay rate γ . Note that this average structure is understood approximately by the classical dynamics [55], with deviations in the semiclassical limit for most γ . We will use numerically determined averages $\langle H \rangle_\gamma(x)$ when analyzing intensity fluctuations in the following.

Comparing Figs. 1 (b) and (c) one observes that in regions with larger average values the individual Husimi functions show larger fluctuations. In order to obtain universality, this suggests to define the scaled Husimi function

$$\tilde{H}_\psi(x) = \frac{H_\psi(x)}{\langle H \rangle_\gamma(x)}, \quad (4)$$

which uses the average Husimi function $\langle H \rangle_\gamma$ for scaling where γ is the decay rate of ψ . The scaled Husimi func-

tions $\tilde{H}_\psi(\mathbf{x})$ appear universal for all γ , showing uniform fluctuations on phase-space, see Fig. 1 (d). This resembles the uniformity of eigenfunctions of closed chaotic quantum maps [18, 19].

For the distribution of scaled intensities we present a conjecture in the next section. Subsequently, we numerically investigate the statistics and present numerical support for the conjecture in Sec. IV.

III. CONJECTURE ON UNIVERSAL INTENSITY STATISTICS

We consider the intensity statistics of resonance states ψ with respect to some arbitrary quantum state φ , i.e., the intensities

$$I_\varphi(\psi) := |\langle \varphi | \psi \rangle|^2. \quad (5)$$

Specific examples are $\varphi = \alpha(\mathbf{x})$ being a coherent state giving the Husimi function, $I_{\alpha(\mathbf{x})}(\psi) \propto H_\psi(\mathbf{x})$, and $\varphi = q$ being a position eigenstate giving the intensity in position space, $I_q(\psi) = |\langle q | \psi \rangle|^2$.

We conjecture for resonance states ψ in chaotic systems with escape that the intensities $I_\varphi(\psi)$ are exponentially distributed with mean value $\mu(\varphi, \gamma)$, depending on the considered φ and the decay rate γ of ψ . Equivalently, the scaled intensities

$$\tilde{I}_\varphi(\psi) = \frac{I_\varphi(\psi)}{\mu(\varphi, \gamma)} \quad (6)$$

are exponentially distributed with mean one,

$$P[\tilde{I}_\varphi(\psi) = w] dw = e^{-w} dw. \quad (7)$$

In particular this means that the statistics of the scaled intensities $\tilde{I}_\varphi(\psi)$ is universal, i.e., independent of the choice of system, φ , and γ . Thus $\tilde{I}_\varphi(\psi)$ shows the same statistics as intensities of eigenfunctions of closed chaotic quantum systems, where an intuitive understanding is well established in terms of a random wave model [8]. Note that similarly one could conjecture a Gaussian distribution of the complex amplitudes $\langle \varphi | \psi \rangle$. We discuss a corresponding random vector model for systems with escape in App. E, which describes the statistics of ψ based on an assumption in one distinguished basis.

We emphasize that the mean values $\mu(\varphi, \gamma)$ are essential for scaling, but they are non-trivial compared to closed systems, where ergodicity implies a uniform mean. It should be possible to relate $\mu(\varphi, \gamma)$ to a semiclassical limit measure for each decay rate γ , in particular if $\varphi = \alpha(\mathbf{x})$ is a coherent state on phase space. However, typically these semiclassical limit measures are just approximately known [55] and are multifractal without smooth phase-space densities.

IV. NUMERICAL RESULTS

In the following we present numerical support for the above conjecture on intensity statistics for systems with escape. This

is done in Sec. IV A for the standard map and in Sec. IV B for the triadic baker map with partial escape, where in both cases the mean $\mu(\varphi, \gamma)$ is numerically approximated. In Sec. IV C a random matrix model is considered, where the mean $\mu(\varphi, \gamma)$ is analytically determined.

A. Standard map with partial escape

For the numerical approximation of the mean intensity $\mu(\varphi, \gamma)$ it is necessary to define which resonance states are used for averaging. On one hand they should have approximately the same decay rate due to the strong dependence of their structure on γ , see Fig. 1 (b). On the other hand the number n_{avg} of considered states should be large enough, such that the average is not too much distorted by fluctuations of individual states. This finite sample effect would lead to deviations from the exponential distribution, see App. C. In order to scale a state ψ with decay rate γ , we choose $n_{\text{avg}} = 200$ for $1/h = 16000$, selecting the closest $n_{\text{avg}}/2$ states with decay rates greater and smaller than γ , respectively.

For the standard map with escape we focus on the intensity statistics of the Husimi function. We first consider the distribution for fixed phase-space points \mathbf{x} using a large range of decay rates γ . Secondly, we investigate the statistics fixing γ and considering many phase-space points. Note that fixing both γ and \mathbf{x} would lead to much less intensity values and thus be insufficient to critically test for the exponential distribution.

First, we investigate the scaled Husimi functions \tilde{H}_ψ for three phase-space points \mathbf{x} . For this purpose we consider all resonance states ψ from the natural decay rate up to close to the inverse decay rate. Note that we exclude $n_{\text{avg}}/2$ resonance states at each end of the decay rate distribution, for which the number of surrounding resonance states is not sufficient for

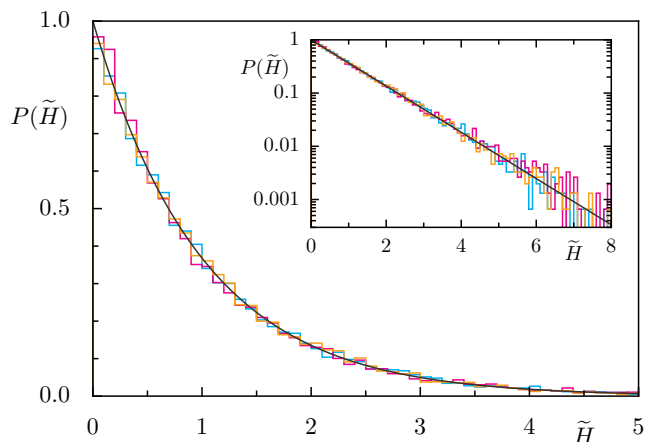


Figure 2. Distribution of scaled Husimi functions \tilde{H}_ψ at three phase-space points $\mathbf{x} = (q, p) \in \{(0.1, 0.2), (0.5, 0.5), (0.8, 0.7)\}$ using $n_{\text{avg}} = 200$ and $1/h = 16000$. Resonance states with decay rates $\gamma \in [\gamma_{\text{nat}}, \gamma_{\text{inv}} - 0.1]$ are used. The exponential distribution with mean one, Eq. (7), is shown as a black line. The inset shows the comparison on a semi-logarithmic scale. The system is the chaotic standard map with partial escape, see App. A.

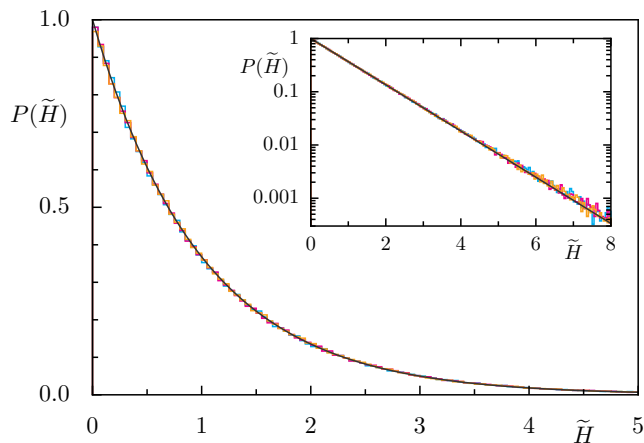


Figure 3. Distribution of scaled Husimi functions \tilde{H}_ψ close to three decay rates $\gamma_{\text{nat}} \approx 0.22$, $\gamma_{\text{typ}} \approx 0.48$, and $\gamma_{\text{inv}} - 0.1 \approx 0.78$ for $n_s = 300$ resonance states each, evaluated on a 50×50 phase-space grid using $n_{\text{avg}} = 200$ and $1/h = 16000$. The exponential distribution with mean one, Eq. (7), is shown as a black line. The inset shows the comparison on a semi-logarithmic scale. The system is the chaotic standard map with partial escape, see App. A.

the computation of the average. The intensity distribution is shown in Fig. 2. It nicely follows the exponential distribution, Eq. (7), with no statistically significant deviations for all three chosen phase-space points, supporting the conjecture.

Secondly, we consider for each of the three decay rates γ_{nat} , γ_{typ} , and $\gamma_{\text{inv}} - 0.1$ a sample of $n_s = 300$ scaled Husimi functions with close-by decay rates γ . They are calculated on a phase-space grid of size 50×50 , which for $1/h = 16000$ has negligible intensity correlations of neighboring points. Their intensity distribution is shown in Fig. 3. It follows the exponential distribution, Eq. (7), with no statistically significant deviations for all three decay rates, again supporting the conjecture.

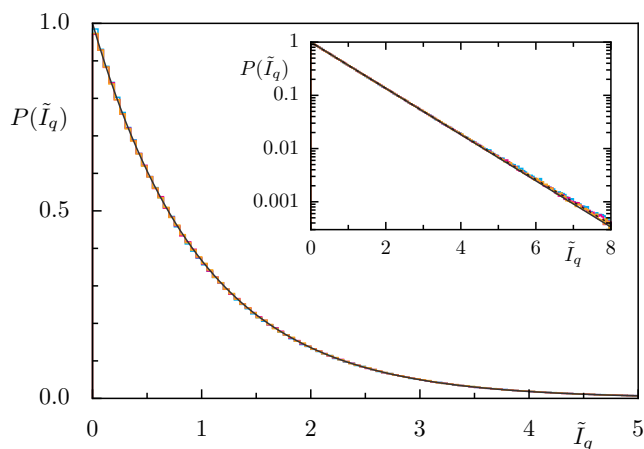


Figure 4. Distribution of scaled position intensities $\tilde{I}_q(\psi)$ for all 16000 positions q , using the same parameters as in Fig. 3. The dashed line in the inset shows additionally the expected distribution when scaling with an average for finite $n_{\text{avg}} = 200$, Eq. (C4).

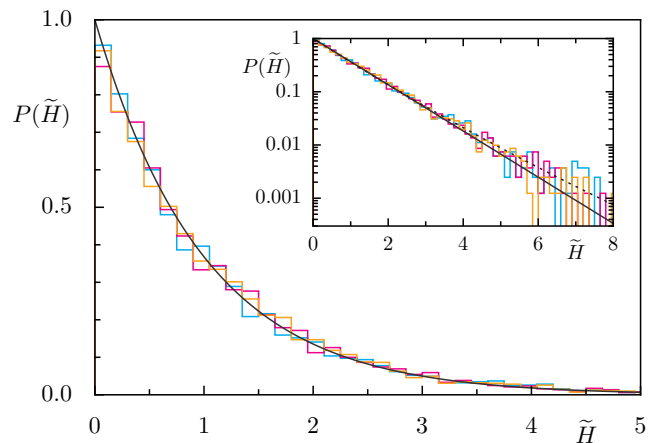


Figure 5. Distribution of scaled Husimi functions \tilde{H}_ψ for $h = 1/250$, $n_{\text{avg}} = n_s = 24$, and considering a 15×15 phase-space grid, otherwise as in Fig. 3. The dashed line in the inset shows additionally the expected distribution when scaling with an average for finite $n_{\text{avg}} = 24$, Eq. (C4).

In order to validate the conjecture in a different basis we illustrate the distribution of scaled position intensities $\tilde{I}_q(\psi)$ in Fig. 4, where the same parameters as in Fig. 3 are used. The intensity distribution nicely follows the exponential distribution, Eq. (7). The inset reveals for large $\tilde{I}_q(\psi) > 6$ a small systematic deviation, which we attribute to scaling by an average using finite n_{avg} , see App. C. This systematic deviation is visible, as the fluctuations are smaller than in Fig. 3.

Let us finally investigate if the intensity statistics follows the conjecture in the quantum regime for larger h . For this we consider scaled Husimi functions \tilde{H}_ψ of resonance states for $h = 1/250$. Since the number of resonance states is much smaller in sufficiently small γ -intervals, we use $n_{\text{avg}} = 24$ and $n_s = 24$. The intensity distribution is shown in Fig. 5. It nicely follows the exponential distribution, Eq. (7), with larger fluctuations than for $h = 1/16000$, as expected. For $\tilde{I}_q(\psi) > 6$ the distribution deviates from the exponential behavior, which we attribute to scaling by an average using finite n_{avg} , see App. C. Thus even towards the quantum regime we find support of the conjecture.

Let us mention that we find numerical support for the conjecture for several reflectivity functions, by varying the region and strength of escape, see App. A. We also confirmed the conjecture for the case of a region with full escape, where the semiclassical support of resonance states converges to the so-called backward trapped set [48], such that one has to restrict the analysis to phase-space points in this set (not shown).

B. Baker map with partial escape

In this section we present results for the baker map with escape which is a well-studied model for chaotic resonances [40, 48–50, 64, 65], defined in App. B. The classical baker map is ergodic, uniformly hyperbolic, and explicit expressions for all periodic orbits are available. For the mean intensity of

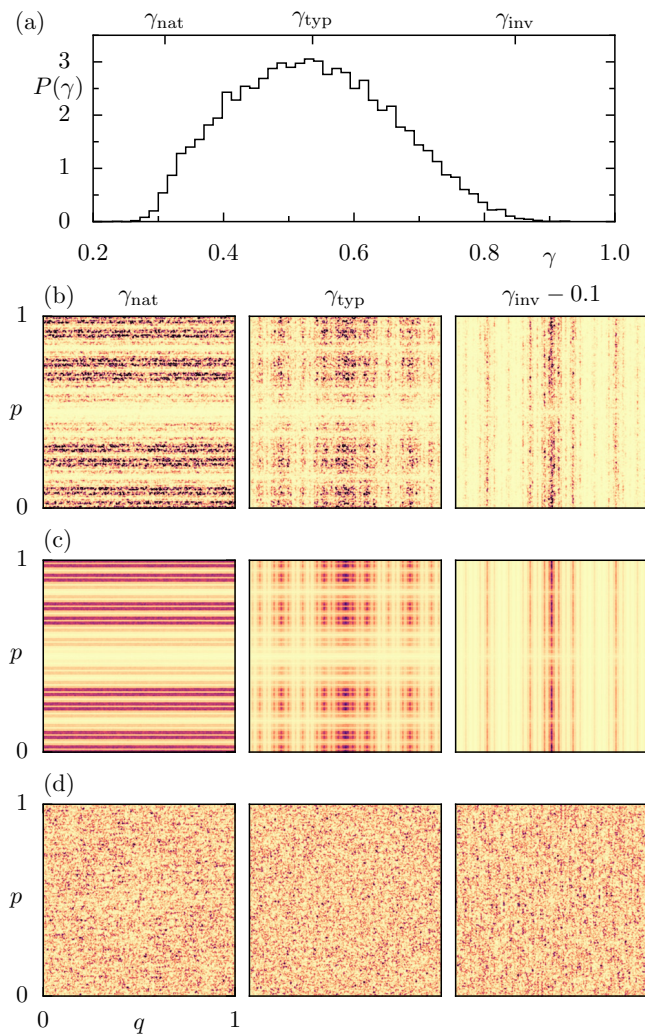


Figure 6. Same as Fig. 1 for the triadic baker map with partial escape, defined in App. B, using $h = 1/16002$. The classical decay rates are $\gamma_{\text{nat}} \approx 0.31$, $\gamma_{\text{typ}} \approx 0.54$, and $\gamma_{\text{inv}} \approx 0.85$.

resonance states a sufficiently accurate classical description is not known and we use numerical approximations, as for the standard map.

In Fig. 6 we show single, average and scaled Husimi functions for three different decay rates γ for the triadic baker map with partial escape at $h = 1/16002$. The single and average Husimi functions reveal a structural change with increasing γ from extending along the classical unstable q -direction to the stable p -direction [55]. The scaled Husimi functions fluctuate uniformly on phase space. Their intensity statistics is shown in Fig. 7 and follows the exponential distribution, Eq. (7), with no statistically significant deviations for all three decay rates, again supporting the conjecture. Similar results for an asymmetric baker map with partial escape are shown in App. B.

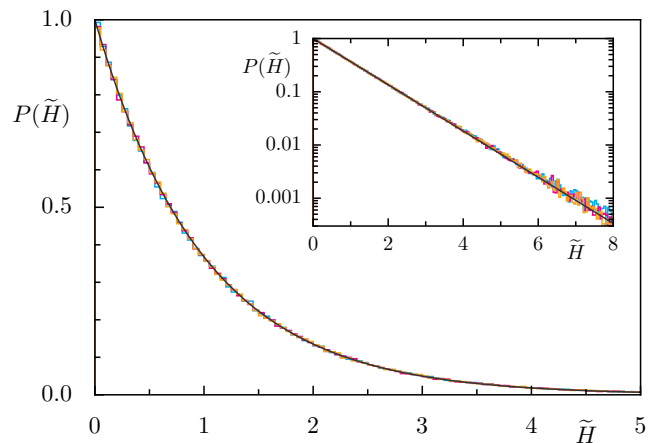


Figure 7. Distribution of scaled Husimi functions \tilde{H}_ψ , for the triadic baker map with partial escape, defined in App. B, using $h = 1/16002$ and considering a 60×60 phase-space grid. Otherwise parameters as in Fig. 3. The considered decay rates are $\gamma_{\text{nat}} \approx 0.31$, $\gamma_{\text{typ}} \approx 0.54$, and $\gamma_{\text{inv}} - 0.1 \approx 0.75$.

C. Random matrix model with partial escape

In this section we introduce a random matrix model with escape and numerically support the conjecture. The motivation for this model is (i) that the mean intensity $\mu(\varphi, \gamma)$ can be described analytically and (ii) that it should allow for a rigorous proof of the conjecture. Note, that the phase-space distribution of resonance states in this model is not multifractal.

We replace the propagator \hat{U} in Eq. (1) with a random matrix \hat{U}^{cue} of dimension N taken from the circular unitary ensemble [70, 71]. The eigenstates of $\hat{U}_r^{\text{cue}} = \hat{U}^{\text{cue}} \hat{R}$ have a much simpler phase-space structure than in systems with deterministic dynamics, depending on the decay rate γ and the reflectivity function $r(\mathbf{x})$. For such a system the mean intensities $\mu(\alpha(\mathbf{x}), \gamma)$ on phase space or $\mu(q, \gamma)$ in position space are given by classical densities $\rho_\gamma(\mathbf{x})$ and $\rho_\gamma(q)$, respectively. A derivation of these densities is given in App. D.

Numerical results are presented for an exemplary smooth reflectivity function, $r(q, p) = 1 - (1 - \alpha) \sin^2(\pi q)$ with $\alpha = 0.05$, see inset of Fig. 8 (a). The distribution of decay rates γ , see Fig. 8 (a), extends approximately from the natural to the inverse decay rate. The intensity in position representation of resonance states for three different decay rates is shown in Fig. 8 (b). These intensities fluctuate around the smooth classical densities ρ_γ , shown for comparison. Averaging over several resonance states with close-by decay rates (or local averaging in position space) we find for large matrix dimension N perfect agreement with the classical density for the natural and inverse natural decay as well as for decay rates in between (not shown). We scale the intensities $I_q(\psi)$ with the classical densities, i.e., using $\mu(q, \gamma) = \rho_\gamma(q)/N$. The scaled intensity $\tilde{I}_q(\psi)$ seems to be independent of the position q and decay rate γ , see Fig. 8 (c), illustrating the universality. The conjectured exponential distribution, Eq. (7), is validated in Fig. 9.

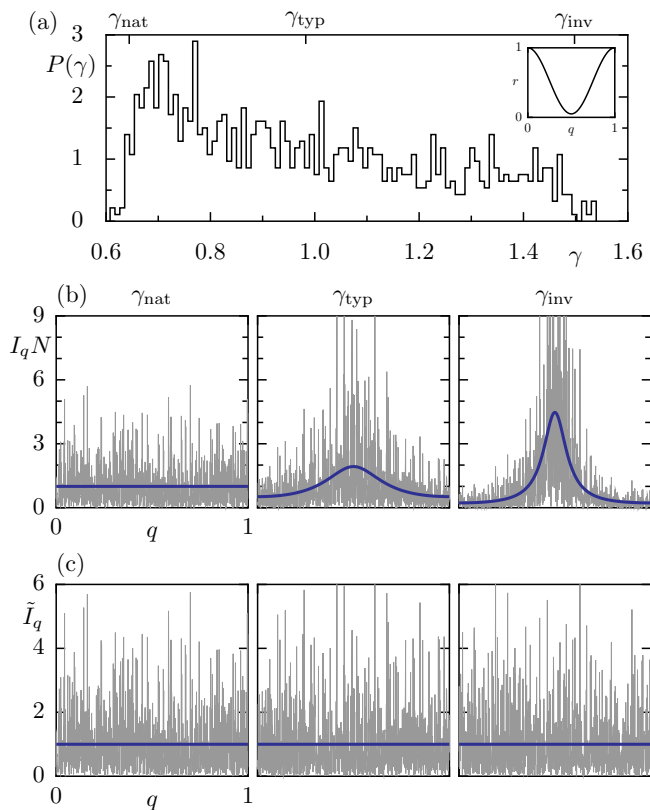


Figure 8. (a) Distribution of quantum decay rates γ for a random matrix with partial escape using $N = 1000$. The inset shows the considered reflectivity function $r(q)$. The classical decay rates $\gamma_{\text{nat}} \approx 0.64$, $\gamma_{\text{typ}} \approx 0.98$, $\gamma_{\text{inv}} \approx 1.5$ are indicated. (b) Intensities in position space $I_q(\psi)N$ for three exemplary resonance states ψ with decay rates γ_{nat} , γ_{typ} , and γ_{inv} and classical density $\rho_\gamma(q)$, Eq. (D10) (thick line). (c) Scaled intensities $\tilde{I}_q(\psi)$ for the same decay rates, compared to the uniform density (thick line).

V. CONCLUSION AND OUTLOOK

In summary, we conjecture that the fluctuations of scaled intensities for resonance states in chaotic quantum systems with escape are universally described by the exponential distribution with mean one. This generalizes well-known results for closed chaotic systems. Numerically we investigate the statistics of single resonance states for the chaotic standard map and the triadic baker map, which are suitably scaled by their respective γ -dependent multifractal average. The Husimi statistics for all considered cases of different phase-space points and decay rates agrees excellently with the conjectured exponential distribution. We demonstrate the conjecture in position basis, deep in the quantum regime for large h , and for different reflectivity functions r . This is further confirmed in a random matrix model with partial escape, for which the semiclassical limit densities of resonance states are derived analytically.

Generic dynamical systems are not fully chaotic, but instead regions of regular and chaotic dynamics coexist. The important question arises whether the conjecture applies to

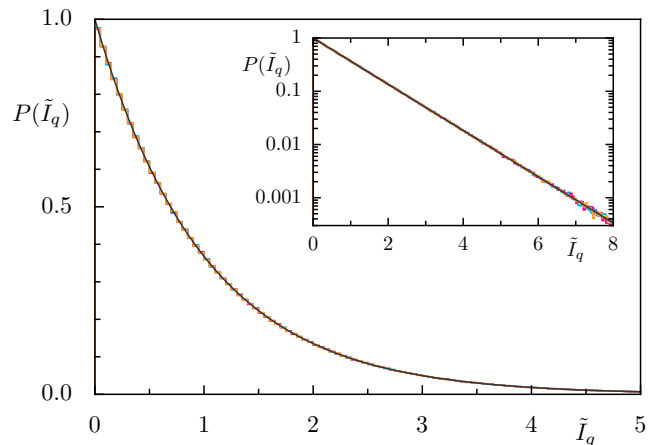


Figure 9. Distribution of scaled intensities $\tilde{I}_q(\psi)$ close to the three decay rates $\gamma_{\text{nat}} \approx 0.64$, $\gamma_{\text{typ}} \approx 0.98$, and $\gamma_{\text{inv}} \approx 1.5$ for $n_s = 300$ resonance states each, evaluated for all position states q for $N = 16000$ using $\rho_\gamma(q)$, Eq. (D10), for scaling. The exponential distribution with mean one, Eq. (7), is shown as a black line. The inset shows the comparison on a semi-logarithmic scale. The system is the random matrix model with partial escape.

such mixed systems with escape. Indeed we find in a preliminary study that the intensity statistics follows the conjecture, if just the subset of chaotic resonance states is considered and if it is investigated just on the chaotic region, while we find no universal statistics for regular resonance states.

The presented analysis does not show signatures of scarring of individual resonances on periodic orbits [62]. In fact, all locally enhanced intensities are consistent with enhancements of the average (which is a multifractal of classical origin) and exponentially distributed fluctuations on top of that. Since the presented statistics involves many resonances, signatures of scarring of individual resonances are possibly concealed. It would be interesting to study the relation between scarring and the observed universal statistics in the future.

There are various further directions in which these results can be generalized: (i) It is interesting to understand if and how different symmetry classes of the closed map and symmetries of the reflectivity function lead to different intensity statistics. (ii) We speculate that the autocorrelation function of scaled Husimi functions behaves as in closed systems [18, 72]. (iii) Another interesting aspect are implications of these results on the fluctuations in the near- and far-field emission of optical microcavities, which are experimentally accessible [56].

ACKNOWLEDGMENTS

We thank J. Keating, S. Nonnenmacher, M. Novaes, S. Prado, and M. Sieber for helpful discussions. This research is funded by the Deutsche Forschungsgemeinschaft (DFG, German Research Foundation) - 262765445.

Appendix A: Standard map with escape

As an example system we consider the paradigmatic standard map on the torus [73], which is given by the time-periodically driven Hamiltonian $H(q, p, t) = p^2/2 + \sum_{n=-\infty}^{\infty} V(q)\delta(t - n)$ with kicking potential $V(q) = \kappa/(4\pi^2)\cos(2\pi q)$ and dimensionless coordinates $(q, p) \in$

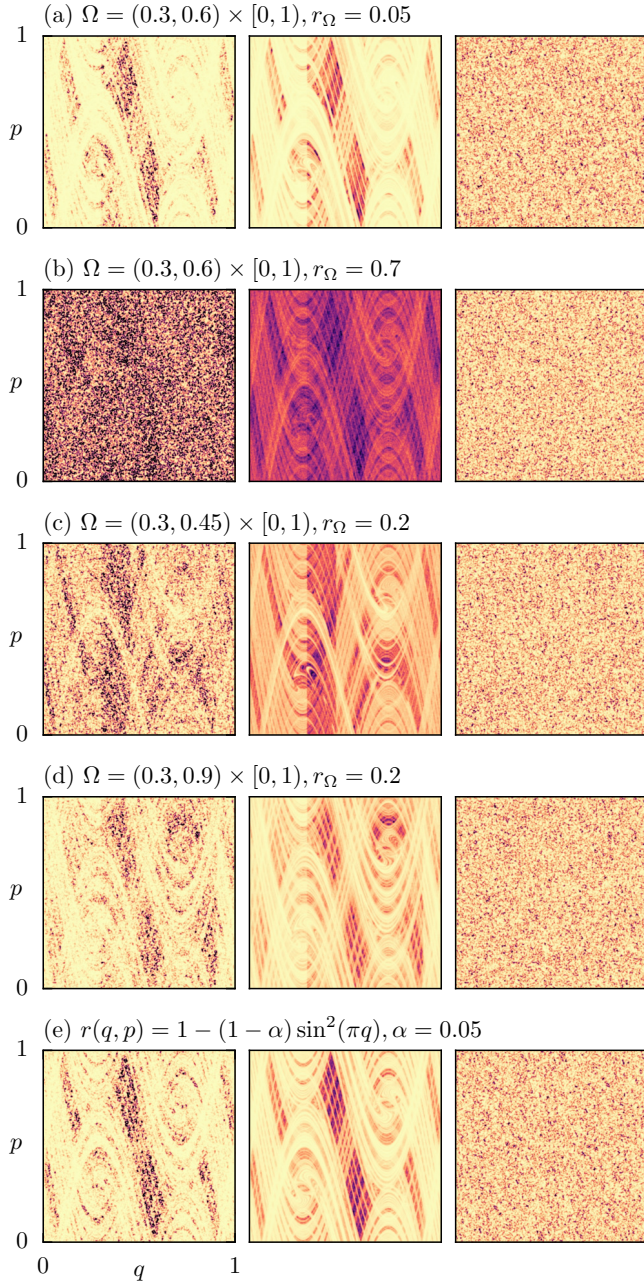


Figure 10. Single H_ψ , averaged $\langle H \rangle_\gamma$, and scaled \tilde{H}_ψ Husimi functions (left to right) for resonance states ψ with decay rate closest to γ_{typ} for the chaotic standard map with different $r(q, p)$, using $h = 1/16000$ and $n_{\text{avg}} = 200$. The typical decay rates are (a) $\gamma_{\text{typ}} \approx 0.90$, (b) $\gamma_{\text{typ}} \approx 0.11$, (c) $\gamma_{\text{typ}} \approx 0.24$, (d) $\gamma_{\text{typ}} \approx 0.97$, and (e) $\gamma_{\text{typ}} \approx 0.98$. Colormaps as in Fig. 1.

$[0, 1) \times [0, 1)$. We consider the half-kick map $M(q, p) = (q + p^*, p - V'(q + p^*)/2)$ with $p^* = p - V'(q)/2$ (similar results are expected for other variants of the map). For $\kappa = 10$ the phase-space contains no visible regular regions, such that we call this setting the chaotic standard map. One possible quantization of this map is given by the unitary propagator between two kicks, which is determined by Floquet quantization [74, 75]. For the half-kick mapping it reads

$$\hat{U} = e^{-i/(2h)V(q)} e^{-i/(2h)p^2} e^{-i/(2h)V(q)}, \quad (\text{A1})$$

where $h = 2\pi\hbar$ takes the role of an effective Planck constant due to dimensionless units q and p . Considering periodic boundary conditions, i.e., dynamics on a torus, only discrete values $h = 1/N$ with $N \in \mathbb{N}$ are allowed. The semiclassical limit is described by $h \rightarrow 0$.

We consider partial escape through some region Ω , such that the reflectivity function is given by $r(q, p) = r_\Omega < 1$ for $(q, p) \in \Omega$ and $r(q, p) = 1$ for $(q, p) \notin \Omega$. This leads to a projective coupling operator [43] of the form $\hat{R} = P_{\Omega^c} + \sqrt{r_\Omega} P_\Omega$. In the main text we use $\Omega = (0.3, 0.6) \times [0, 1)$ and $r_\Omega = 0.2$.

Here we present additional results for different reflectivity functions $r(q, p)$. For this purpose we first consider the same opening Ω and choose two different reflectivities r_Ω leading to much stronger and weaker escape from the system, respectively. Secondly, we choose smaller and larger openings Ω for the same reflectivity r_Ω . Finally, also a smooth reflectivity function is considered. In Fig. 10 for these five different choices of $r(q, p)$ the single, averaged, and scaled Husimi functions for the respective decay rate γ_{typ} are shown. In all cases the scaled Husimi function is uniform on phase space (rightmost panels). The corresponding intensity statistics is shown in Fig. 11. For all considered reflectivity functions it nicely follows the conjectured exponential distribution with no statistically significant deviations.

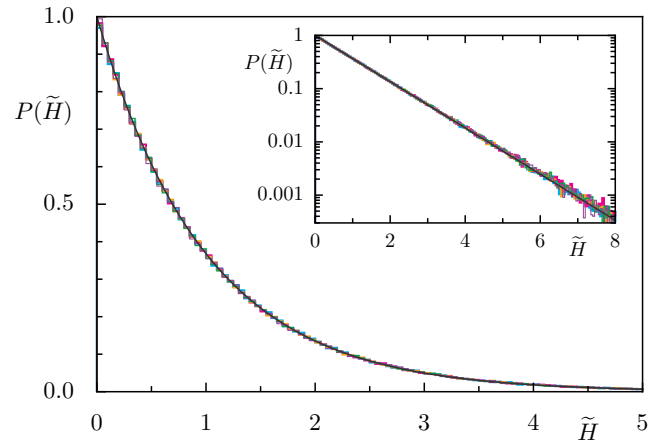


Figure 11. Distribution of scaled Husimi functions \tilde{H}_ψ with decay rates close to γ_{typ} for the chaotic standard map with different $r(q, p)$, as specified in Fig. 10. Other parameters as in Fig. 3.

Appendix B: Baker map with escape

The generalized n -baker map on the two-torus $[0, 1) \times [0, 1)$ is defined as follows [76]. Let $\mathbf{b} \in \mathbb{R}_{>0}^n$ with $\sum_{i=1}^n b_i = 1$ denote the relative size of n vertical rectangles $A_k = [a_k, a_k + b_k) \times [0, 1)$, where $a_k := \sum_{i=1}^{k-1} b_i$ corresponds to the left boundary of A_k (with $a_1 = 0$ and $a_{k+1} = 1$). With this, the baker map is defined as $B_{\mathbf{b}}(q, p) := ((q - a_k)/b_k, b_k p + a_k)$ for $q \in [a_k, a_{k+1})$. I.e., in one step the i -th rectangle is compressed along the p -direction by the factor b_i and stretched along the q -direction by the factor $1/b_i$, after which being stacked on top of each other. The quantized baker map is given by [77, 78]

$$\hat{B}_{\mathbf{b}} = \mathcal{F}_N^{-1} \text{diag}(\mathcal{F}_{N_1}, \mathcal{F}_{N_2}, \dots, \mathcal{F}_{N_n}), \quad (\text{B1})$$

where $[\mathcal{F}_{\mathcal{M}}]_{kl} := M^{-1/2} e^{-2\pi i(k+1/2)(l+1/2)/M}$ denotes the discrete Fourier transform of dimension M , and $N_i/N = b_i$.

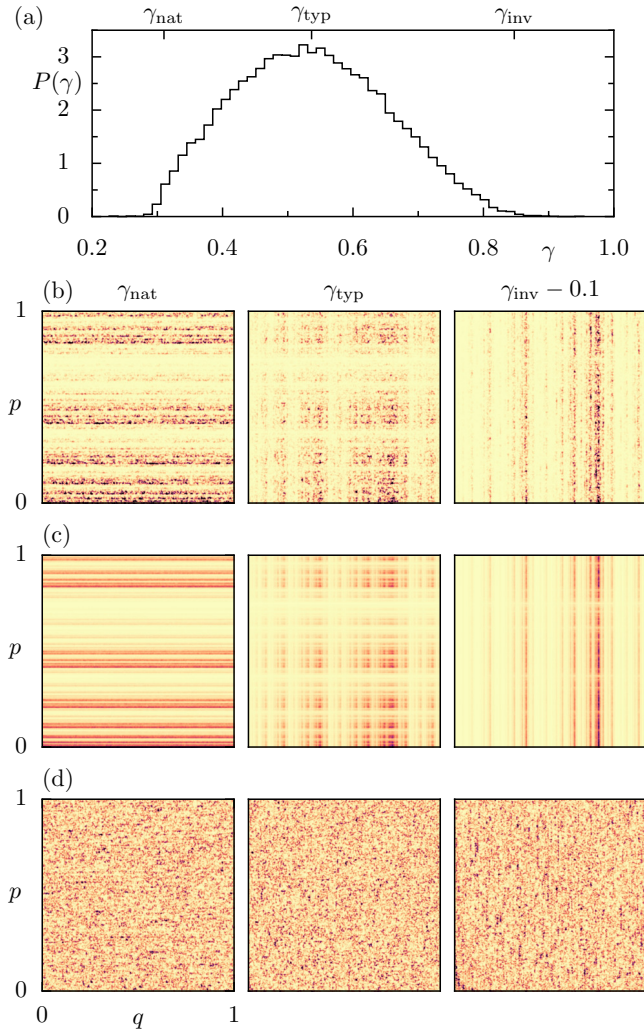


Figure 12. Same as Fig. 1 for the asymmetric baker map with partial escape using $h = 1/16002$. The classical decay rates are $\gamma_{\text{nat}} \approx 0.31$, $\gamma_{\text{typ}} \approx 0.54$, and $\gamma_{\text{inv}} \approx 0.85$.

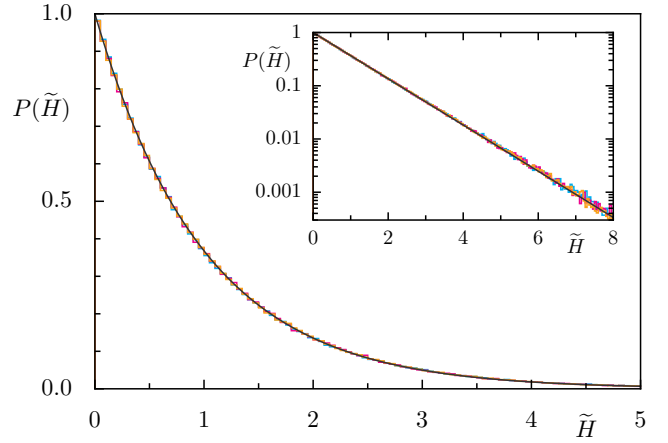


Figure 13. Distribution of scaled Husimi functions \tilde{H}_ψ for the asymmetric baker map with partial escape using $h = 1/16002$ and considering a 60×60 phase-space grid. Other parameters as in Fig. 3. The considered decay rates are $\gamma_{\text{nat}} \approx 0.31$, $\gamma_{\text{typ}} \approx 0.54$, and $\gamma_{\text{inv}} - 0.1 \approx 0.75$.

For the baker map with escape we consider reflectivity functions which are constant in each rectangle, $r(q, p) = r_k$ for $q \in [a_k, a_{k+1})$ for some $\mathbf{r} \in \mathbb{R}_{>0}^n$. This allows to determine the classical decay rates analytically, which gives $\gamma_{\text{nat}} = -\ln \sum_{i=1}^n b_i r_i$, $\gamma_{\text{inv}} = \ln \sum_{i=1}^n b_i / r_i$, and $\gamma_{\text{typ}} = -\sum_{i=1}^n b_i \ln r_i$. In Sec. IV B results are presented for the triadic baker map with equal sizes $\mathbf{b} = (1/3, 1/3, 1/3)$, where escape from the middle strip is considered as $\mathbf{r} = (1, 0.2, 1)$.

Here we show additional results for an asymmetric baker map with escape, defined by $\mathbf{b} = (1/2, 1/3, 1/6)$ and $\mathbf{r} = (1, 0.2, 1)$, see Fig. 12 and Fig. 13.

Appendix C: Deviations from exponential distribution due to scaling with average over finite sample

In this section we derive how the distribution of scaled intensities deviates from the exponential distribution, if a finite sample n_{avg} is used to determine the average. This becomes relevant in situations where the calculation is numerically costly, e.g., in billiards with escape like optical microcavities.

Therefore, we consider intensities which are described by exponentially distributed random variables X_i with the same mean $1/\lambda$. Their probability density function is then given by

$$P(X_i = x) = \Theta(x) \lambda e^{-\lambda x} \quad (\text{C1})$$

Let X_0 denote the random variable that we wish to scale and let $n = n_{\text{avg}}$ be the number of states contributing to the average. Then the random variable

$$Y = \frac{X_0}{\frac{1}{n} \sum_{i=1}^n X_i} \quad (\text{C2})$$

models the scaled intensity, see Eq. (6). Its probability density

function can be calculated as

$$P_n(Y = y) = \int_0^\infty dx_0 \int_0^\infty dx_1 \cdots \int_0^\infty dx_n \quad (\text{C3})$$

$$\delta\left(y - \frac{x_0}{\frac{1}{n} \sum_{i=1}^n x_i}\right) \prod_{i=0}^n P(X_i = x_i) \\ = \left(1 + \frac{y}{n}\right)^{-(n+1)}. \quad (\text{C4})$$

As expected, in the limit of large n this distribution converges to the exponential distribution, $P_n(Y = y) \xrightarrow{n \rightarrow \infty} e^{-y}$. We observe for values of $n < 100$ that the distribution of scaled intensities of resonance states closely follows Eq. (C4) (not shown). For the considered value of $n_{\text{avg}} = 200$ the deviation between Eq. (C4) and the exponential distribution is almost not visible in Figs. 2 and 3, the relative error being about 4% (12%) for $y = 5$ ($y = 8$). Note that it is also possible to include X_0 in the average in Eq. (C2), leading to a slightly different distribution P_n , which converges as well to the exponential distribution for $n \rightarrow \infty$.

Appendix D: Classical densities for random matrix model with partial escape

For the random matrix model with partial escape used in Sec. IV C classical densities $\rho_\gamma(\mathbf{x})$, which we assume to describe the mean intensities of resonance states, are derived as follows. Classically, the natural decay rate γ_{nat} and the natural decay rate from the inverse dynamics, γ_{inv} , as well as their corresponding densities are given by

$$\rho_{\text{nat}}(\mathbf{x}) = 1, \quad e^{-\gamma_{\text{nat}}} = \int r(\mathbf{x}) d\mathbf{x}, \quad (\text{D1})$$

$$\rho_{\text{inv}}(\mathbf{x}) = \frac{1}{e^{\gamma_{\text{inv}}} r(\mathbf{x})}, \quad e^{\gamma_{\text{inv}}} = \int \frac{1}{r(\mathbf{x})} d\mathbf{x}. \quad (\text{D2})$$

These densities are stable under forward (backward) iteration of a corresponding classical time evolution. Here the (inverse) random matrix is replaced by a stochastic map which leads to the uniform density in a single step, while keeping the norm. Specifically, under forward iteration of $\rho_{\text{nat}}(\mathbf{x})$ first the reflectivity function reduces the norm by the factor $e^{-\gamma_{\text{nat}}}$ and the random step makes the density uniform again. Under backward iteration of $\rho_{\text{inv}}(\mathbf{x})$ first the random step leads to the uniform density and then the inverted reflectivity function $1/r(\mathbf{x})$ increases the norm by the factor $e^{\gamma_{\text{inv}}}$ (corresponding in forward direction to a decay by $e^{-\gamma_{\text{inv}}}$) and induces the phase-space density $\rho_{\text{inv}}(\mathbf{x}) \propto 1/r(\mathbf{x})$.

For arbitrary decay rates γ the classical density $\rho_\gamma(\mathbf{x})$ has to fulfill the condition of normalization,

$$\int \rho_\gamma(\mathbf{x}) d\mathbf{x} = 1, \quad (\text{D3})$$

and the condition of decay with γ under forward iteration,

$$\int r(\mathbf{x}) \rho_\gamma(\mathbf{x}) d\mathbf{x} = e^{-\gamma} \int \rho_\gamma(\mathbf{x}) d\mathbf{x}. \quad (\text{D4})$$

This can be equivalently written as

$$\int g_\gamma(\mathbf{x}) \rho_\gamma(\mathbf{x}) d\mathbf{x} = 0, \quad (\text{D5})$$

where

$$g_\gamma(\mathbf{x}) = e^\gamma r(\mathbf{x}) - 1 \quad (\text{D6})$$

is fixed by the considered reflectivity function $r(\mathbf{x})$ and the decay rate γ . There are in general infinitely many classical densities $\rho_\gamma(\mathbf{x})$ satisfying Eq. (D5) and it is not obvious which one is relevant quantum mechanically. We will use that due to linearity the solutions $\rho_\gamma(\mathbf{x})$ of Eq. (D5) are the same when replacing $g_\gamma(\mathbf{x})$ by some function $g(\mathbf{x}) = \xi g_\gamma(\mathbf{x})$ with a factor ξ . According to Eq. (D6) we write this function as

$$\xi g_\gamma(\mathbf{x}) = e^{\gamma_\xi} r_\xi(\mathbf{x}) - 1, \quad (\text{D7})$$

which defines a pair $(r_\xi(\mathbf{x}), \gamma_\xi)$ for any ξ (up to a global factor which keeps the product $e^{\gamma_\xi} r_\xi(\mathbf{x})$ constant and will be irrelevant in the following). For all ξ these pairs describe different reflectivity functions $r_\xi(\mathbf{x})$ and decay rates γ_ξ , but relate to the same function $g_\gamma(\mathbf{x})$ and thus have the same possible classical densities, as seen from Eq. (D5).

We now assume that the specific density relevant for quantum mechanics, i.e., that describes the mean intensity of resonance states with decay rate γ , is the same for all related pairs $(r_\xi(\mathbf{x}), \gamma_\xi)$. This implies that it is sufficient to solve the problem for one particular ξ and the related pair $(r_\xi(\mathbf{x}), \gamma_\xi)$. Furthermore we assume that for $\gamma = \gamma_{\text{inv}}$ the quantum mechanically relevant density is given by the classically stable density $\rho_{\text{inv}}(\mathbf{x})$, Eq. (D2). Applying this assumption to the related pairs $(r_\xi(\mathbf{x}), \gamma_\xi)$, it is thus sufficient to search for a case where γ_ξ is the inverse decay rate corresponding to the reflectivity function $r_\xi(\mathbf{x})$, i.e., $e^{\gamma_\xi} = \int 1/r_\xi(\mathbf{x}) d\mathbf{x}$, see Eq. (D2). This occurs for some specific factor $\xi = \xi^*$ and leads to the density, Eq. (D2),

$$\rho_\gamma(\mathbf{x}) = \frac{1}{e^{\gamma_\xi^*} r_{\xi^*}(\mathbf{x})} = \frac{1}{1 + \xi^* g_\gamma(\mathbf{x})}, \quad (\text{D8})$$

where the second equality follows from Eq. (D7). The factor ξ^* is uniquely determined from the condition on the decay of the density, Eq. (D5),

$$\int \frac{g_\gamma(\mathbf{x})}{1 + \xi^* g_\gamma(\mathbf{x})} d\mathbf{x} = 0. \quad (\text{D9})$$

Uniqueness follows from the negative derivative with respect to ξ^* and existence can be shown for classically allowed decay rates, $\min r(\mathbf{x}) \leq e^{-\gamma} \leq \max r(\mathbf{x})$. We emphasize that ξ^* depends on $r(\mathbf{x})$ and γ .

Summarizing, based on our assumptions the classical density

$$\rho_\gamma(\mathbf{x}) = \frac{1}{1 + \xi^* g_\gamma(\mathbf{x})} \quad (\text{D10})$$

describes the mean intensity of resonance states with decay rate γ in the random matrix model with escape, where $g_\gamma(\mathbf{x})$

is defined in Eq. (D6) and ξ^* is determined from Eq. (D9). The special cases, $\xi^*(\gamma_{\text{nat}}) = 0$ and $\xi^*(\gamma_{\text{inv}}) = 1$, agree with Eqs. (D1) and (D2), respectively. Note that if there is a phase-space region with full escape, $r(\mathbf{x}) = 0$, then $\gamma_{\text{inv}} = \infty$, but for $\gamma < \infty$ Eq. (D10) still applies.

We numerically find that resonance states of the random matrix model converge towards the densities $\rho_\gamma(\mathbf{x})$ as N increases (not shown). This has been tested for several reflectivity functions $r(\mathbf{x})$, varying on phase space and including cases where both full and partial escape occur in different phase-space regions.

Appendix E: Random vector model for partial escape

In this section we present a random vector model for systems with partial escape. The goal is a statistical description of the complex vector ψ . This is achieved by assuming independently distributed Gaussian complex entries in only one distinguished basis. In the following we will see that the random vector model implies the conjecture of Sec. III for intensities with respect to any quantum state φ .

First, let us consider the simplest setting of random matrices with escape \hat{U}_r^{cue} , introduced in Sec. IV C. Without loss of generality we assume that $r(\mathbf{x})$ is a function of position q only, such that $\hat{R} = \text{Op}_N \sqrt{r}$ can be chosen diagonal in position basis. This implies, according to Eq. (D10), that for all γ the semiclassical densities $\rho_\gamma(\mathbf{x})$ also depend on q , only. Thus, quantizing the classical densities leads to a diagonal representation in position basis.

We propose the following random vector model for the distribution of coefficients of resonance states ψ for some arbitrary, but fixed decay rate γ . Let $\psi_j = \langle q_j | \psi \rangle$ be the coefficients in position basis, such that $|\psi\rangle = \sum_{j=1}^N \psi_j |q_j\rangle$. For this, the expected mean value of the intensities $I_{q_j}(\psi) = |\psi_j|^2$ is given by $\rho_\gamma(q_j)/N$. This leads to the following adaptation of the CUE ensemble of random states [18]: For any fixed decay rate γ we define the ensemble of random vectors $\psi = (\psi_1, \dots, \psi_N)$ as

$$P_\gamma(\psi) \prod_{j=1}^N d^2\psi_j = \prod_{j=1}^N \left(\frac{N}{\pi \rho_\gamma(q_j)} \exp \left[-\frac{N |\psi_j|^2}{\rho_\gamma(q_j)} \right] \right) d^2\psi_j, \quad (\text{E1})$$

where the complex coefficients ψ_j are independent and identically distributed according to a Gaussian with variance $\rho_\gamma(q_j)/N$. For each γ this definition ensures that the ex-

pectation value $\mathbb{E}_\gamma(|\psi_j|^2)$ is given by $\rho_\gamma(q_j)/N$ and that on average we have normalized states, i.e., $\mathbb{E}_\gamma(\sum_j |\psi_j|^2) = \sum_j \rho_\gamma(q_j)/N = 1$. Note that such a position dependent variance also follows from the restricted random vector model describing quantum maps with a mixed phase space [21].

In order to derive for some arbitrary quantum state φ the distribution of intensities $I_\varphi(\psi)$, Eq. (5), we consider the overlap $\nu_\varphi = \langle \varphi | \psi \rangle$. Since Eq. (E1) describes a (circularly-symmetric) complex normal distribution with diagonal covariance matrix $C_\gamma = N^{-1} \text{diag}[\rho_\gamma(q_1), \dots, \rho_\gamma(q_N)]$ it follows that ν_φ is also normally distributed with variance given by $C_{\gamma,\varphi} = \langle \varphi | C_\gamma | \varphi \rangle = N^{-1} \sum_{j=1}^N \rho_\gamma(q_j) |\langle q_j | \varphi \rangle|^2$ [79], i.e.,

$$P_\gamma(\nu) d^2\nu = \frac{1}{\pi C_{\gamma,\varphi}} \exp \left(-\frac{|\nu|^2}{C_{\gamma,\varphi}} \right) d^2\nu. \quad (\text{E2})$$

This implies directly that $I_\varphi(\psi) = |\nu|^2$ is exponentially distributed with mean value $\mu(\varphi, \gamma) = C_{\gamma,\varphi}$, i.e., the conjecture stated in Sec. III.

In general $r(\mathbf{x})$ might depend on q and p , such that \hat{R} is diagonal in some different basis $\{b_i\}_{i=1}^N$ with eigenvalues w_i . However, transforming \hat{U}_r^{cue} to this basis, $\hat{B}^\dagger \hat{U}_r^{\text{cue}} \hat{R} \hat{B} = \hat{V}^{\text{cue}} \hat{R}_{\text{diag}}$, implies a random matrix $\hat{V}^{\text{cue}} := \hat{B}^\dagger \hat{U}_r^{\text{cue}} \hat{B}$ with diagonal reflection operator $\hat{R}_{\text{diag}} = \text{diag}(w_1, \dots, w_N)$ which can be treated as before. The expected mean value of the intensities $I_{b_j}(\psi) = |\langle b_j | \psi \rangle|^2$ for resonance states of \hat{U}_r^{cue} thus is given by $\rho_\gamma(b_i)/N$ where $\rho_\gamma(b_i) = [1 + \xi_\gamma(e^\gamma \tilde{r}_i - 1)]^{-1}$ and $\tilde{r}_i = |w_i|^2$.

Finally, let us discuss how this random vector model could be extended to arbitrary chaotic systems with escape. There are three major challenges: (i) The semiclassical structure of resonance states in arbitrary systems is a multifractal measure without density. (ii) A complete semiclassical description of these measures is still missing. (iii) For each decay rate γ we expect a different basis for the distribution in Eq. (E1).

For fluctuations on phase space, the first issue is overcome by the fact that the quantum Husimi densities are smooth functions. Thus, for fixed value of h their expected mean value also behaves smoothly on phase space. Therefore, together with the second challenge, this reduces to the problem of obtaining the correct smooth density from the semiclassical multifractal measure. The third issue is caused by the change of the phase-space structure under variation of γ [55], see Fig. 1. Thus the mean densities ρ_γ do not have a quantum mechanically diagonal representation in the same basis for different decay rates. Therefore, in contrast to the random model with escape, it would be necessary to first obtain the specific basis for each γ .

[1] A. I. Shnirelman, Ergodic properties of eigenfunctions (in Russian), *Usp. Math. Nauk* **29**, 181 (1974).
[2] Y. Colin de Verdière, Ergodicité et fonctions propres du laplacien (in French), *Commun. Math. Phys.* **102**, 497 (1985).
[3] S. Zelditch, Uniform distribution of eigenfunctions on compact hyperbolic surfaces, *Duke. Math. J.* **55**, 919 (1987).

[4] S. Zelditch and M. Zworski, Ergodicity of eigenfunctions for ergodic billiards, *Commun. Math. Phys.* **175**, 673 (1996).
[5] A. Bäcker, R. Schubert, and P. Stifter, Rate of quantum ergodicity in Euclidean billiards, *Phys. Rev. E* **57**, 5425 (1998), ; erratum *ibid.* **58** (1998) 5192.
[6] M. Degli Esposti, S. Graffi, and S. Isola, Classical limit

- of the quantized hyperbolic toral automorphisms, *Commun. Math. Phys.* **167**, 471 (1995).
- [7] A. Bouzouina and S. De Bièvre, Equipartition of the eigenfunctions of quantized ergodic maps on the torus, *Commun. Math. Phys.* **178**, 83 (1996).
- [8] M. V. Berry, Regular and irregular semiclassical wavefunctions, *J. Phys. A* **10**, 2083 (1977).
- [9] S. W. McDonald and A. N. Kaufman, Wave chaos in the stadium: Statistical properties of short-wave solutions of the Helmholtz equation, *Phys. Rev. A* **37**, 3067 (1988).
- [10] R. Aurich and F. Steiner, Exact theory for the quantum eigenstates of a strongly chaotic system, *Physica D* **48**, 445 (1991).
- [11] B. Li and M. Robnik, Statistical properties of high-lying chaotic eigenstates, *J. Phys. A* **27**, 5509 (1994).
- [12] T. Prosen, Quantization of generic chaotic 3D billiard with smooth boundary II: Structure of high-lying eigenstates, *Phys. Lett. A* **233**, 332 (1997).
- [13] T. A. Brody, J. Flores, J. B. French, P. A. Mello, A. Pandey, and S. S. M. Wong, Random-matrix physics: spectrum and strength fluctuations, *Rev. Mod. Phys.* **53**, 385 (1981).
- [14] T. Guhr, A. Müller-Groeling, and H. A. Weidenmüller, Random-matrix theories in quantum physics: common concepts, *Phys. Rep.* **299**, 189 (1998).
- [15] F. M. Izrailev, Chaotic structure of eigenfunctions in systems with maximal quantum chaos, *Phys. Lett. A* **125**, 250 (1987).
- [16] K. Życzkowski and G. Lenz, Eigenvector statistics for the transitions from the orthogonal to the unitary ensemble, *Z. Phys. B* **82**, 299 (1991).
- [17] M. Kuś, J. Mostowski, and F. Haake, Universality of eigenvector statistics of kicked tops of different symmetries, *J. Phys. A* **21**, L1073 (1988).
- [18] S. Nonnenmacher and A. Voros, Chaotic eigenfunctions in phase space, *J. Stat. Phys.* **92**, 431 (1998).
- [19] A. Bäcker, Numerical aspects of eigenvalues and eigenfunctions of chaotic quantum systems, in [80], pp. 91–144.
- [20] A. Bäcker and R. Schubert, Amplitude distribution of eigenfunctions in mixed systems, *J. Phys. A* **35**, 527 (2002).
- [21] A. Bäcker and S. Nonnenmacher, Restricted random vector models and eigenvector statistics in systems with a mixed phase space, in preparation.
- [22] W. E. Bies, N. Lepore, and E. J. Heller, Quantum billiards and constrained random wave correlations, *J. Phys. A* **36**, 1605 (2003).
- [23] J. D. Urbina and K. Richter, Supporting random wave models: a quantum mechanical approach, *J. Phys. A* **36**, L495 (2003).
- [24] J. D. Urbina and K. Richter, Statistical description of eigenfunctions in chaotic and weakly disordered systems beyond universality, *Phys. Rev. Lett.* **97**, 214101 (2006).
- [25] A. De Luca and A. Scardicchio, Ergodicity breaking in a model showing many-body localization, *Europhys. Lett.* **101**, 37003 (2013).
- [26] W. Beugeling, A. Bäcker, R. Moessner, and M. Haque, Statistical properties of eigenstate amplitudes in complex quantum systems, *Phys. Rev. E* **98**, 022204 (2018).
- [27] A. Bäcker, M. Haque, and I. M. Khaymovich, Multifractal dimensions for random matrices, chaotic quantum maps, and many-body systems, *Phys. Rev. E* **100**, 032117 (2019).
- [28] E. G. Altmann, J. S. E. Portela, and T. Tél, Leaking chaotic systems, *Rev. Mod. Phys.* **85**, 869 (2013).
- [29] P. Gaspard and S. A. Rice, Exact quantization of the scattering from a classically chaotic repeller, *J. Chem. Phys.* **90**, 2255 (1989).
- [30] A. Wirzba, Quantum mechanics and semiclassics of hyperbolic n -disk scattering systems, *Phys. Rep.* **309**, 1 (1999).
- [31] T. Weich, S. Barkhofen, U. Kuhl, C. Poli, and H. Schomerus, Formation and interaction of resonance chains in the open three-disk system, *New J. Phys.* **16**, 033029 (2014).
- [32] H. Cao and J. Wiersig, Dielectric microcavities: Model systems for wave chaos and non-Hermitian physics, *Rev. Mod. Phys.* **87**, 61 (2015).
- [33] J. Sjöstrand, Geometric bounds on the density of resonances for semiclassical problems, *Duke Math. J.* **60**, 1 (1990).
- [34] K. K. Lin, Numerical study of quantum resonances in chaotic scattering, *J. Comput. Phys.* **176**, 295 (2002).
- [35] W. T. Lu, S. Sridhar, and M. Zworski, Fractal Weyl laws for chaotic open systems, *Phys. Rev. Lett.* **91**, 154101 (2003).
- [36] H. Schomerus and J. Tworzydło, Quantum-to-classical crossover of quasibound states in open quantum systems, *Phys. Rev. Lett.* **93**, 154102 (2004).
- [37] J. A. Ramiłowski, S. D. Prado, F. Borondo, and D. Farrelly, Fractal Weyl law behavior in an open Hamiltonian system, *Phys. Rev. E* **80**, 055201(R) (2009).
- [38] A. Eberspächer, J. Main, and G. Wunner, Fractal Weyl law for three-dimensional chaotic hard-sphere scattering systems, *Phys. Rev. E* **82**, 046201 (2010).
- [39] L. Ermann and D. L. Shepelyansky, Ulam method and fractal Weyl law for Perron-Frobenius operators, *Eur. Phys. J. B* **75**, 299 (2010).
- [40] J. M. Pedrosa, D. Wisniacki, G. G. Carlo, and M. Novaes, Short periodic orbit approach to resonances and the fractal Weyl law, *Phys. Rev. E* **85**, 036203 (2012).
- [41] S. Nonnenmacher, J. Sjöstrand, and M. Zworski, Fractal Weyl law for open quantum chaotic maps, *Ann. Math.* **179**, 179 (2014).
- [42] J. Wiersig and J. Main, Fractal Weyl law for chaotic microcavities: Fresnel's laws imply multifractal scattering, *Phys. Rev. E* **77**, 036205 (2008).
- [43] S. Nonnenmacher and E. Schenck, Resonance distribution in open quantum chaotic systems, *Phys. Rev. E* **78**, 045202(R) (2008).
- [44] B. Gutkin and V. A. Osipov, Universality in spectral statistics of open quantum graphs, *Phys. Rev. E* **91**, 060901(R) (2015).
- [45] M. Schönwetter and E. G. Altmann, Quantum signatures of classical multifractal measures, *Phys. Rev. E* **91**, 012919 (2015).
- [46] G. Casati, G. Maspero, and D. L. Shepelyansky, Quantum fractal eigenstates, *Physica D* **131**, 311 (1999).
- [47] S.-Y. Lee, S. Rim, J.-W. Ryu, T.-Y. Kwon, M. Choi, and C.-M. Kim, Quasiscattered resonances in a spiral-shaped microcavity, *Phys. Rev. Lett.* **93**, 164102 (2004).
- [48] J. P. Keating, M. Novaes, S. D. Prado, and M. Sieber, Semiclassical structure of chaotic resonance eigenfunctions, *Phys. Rev. Lett.* **97**, 150406 (2006).
- [49] S. Nonnenmacher and M. Rubin, Resonant eigenstates for a quantized chaotic system, *Nonlinearity* **20**, 1387 (2007).
- [50] J. P. Keating, S. Nonnenmacher, M. Novaes, and M. Sieber, On the resonance eigenstates of an open quantum baker map, *Nonlinearity* **21**, 2591 (2008).
- [51] T. Harayama and S. Shinohara, Ray-wave correspondence in chaotic dielectric billiards, *Phys. Rev. E* **92**, 042916 (2015).
- [52] M. J. Körber, A. Bäcker, and R. Ketzmerick, Localization of chaotic resonance states due to a partial transport barrier, *Phys. Rev. Lett.* **115**, 254101 (2015).
- [53] J. Kullig and J. Wiersig, Frobenius–Perron eigenstates in deformed microdisk cavities: non-Hermitian physics and asymmetric backscattering in ray dynamics, *New J. Phys.* **18**, 015005 (2016).
- [54] K. Clauß, M. J. Körber, A. Bäcker, and R. Ketzmer-

- ick, Resonance eigenfunction hypothesis for chaotic systems, *Phys. Rev. Lett.* **121**, 074101 (2018).
- [55] K. Clauß, E. G. Altmann, A. Bäcker, and R. Ketzmerick, Structure of resonance eigenfunctions for chaotic systems with partial escape, *Phys. Rev. E* **100**, 052205 (2019).
- [56] S. Bittner, K. Kim, Y. Zeng, Q. J. Wang, and H. Cao, Spatial structure of lasing modes in wave-chaotic semiconductor microcavities, *New J. Phys.* **22**, 083002 (2020).
- [57] M. F. Demers and L.-S. Young, Escape rates and conditionally invariant measures, *Nonlinearity* **19**, 377 (2006).
- [58] E. J. Heller, Bound-state eigenfunctions of classically chaotic Hamiltonian systems: Scars of periodic orbits, *Phys. Rev. Lett.* **53**, 1515 (1984).
- [59] W. Fang, A. Yamilov, and H. Cao, Analysis of high-quality modes in open chaotic microcavities, *Phys. Rev. A* **72**, 023815 (2005).
- [60] J. Wiersig, Formation of long-lived, scarlike modes near avoided resonance crossings in optical microcavities, *Phys. Rev. Lett.* **97**, 253901 (2006).
- [61] J. Wiersig and M. Hentschel, Combining directional light output and ultralow loss in deformed microdisks, *Phys. Rev. Lett.* **100**, 033901 (2008).
- [62] D. Wisniacki and G. G. Carlo, Scarring in open quantum systems, *Phys. Rev. E* **77**, 045201(R) (2008).
- [63] L. Ermann, G. G. Carlo, and M. Saraceno, Localization of resonance eigenfunctions on quantum repellers, *Phys. Rev. Lett.* **103**, 054102 (2009).
- [64] M. Novaes, J. M. Pedrosa, D. Wisniacki, G. G. Carlo, and J. P. Keating, Quantum chaotic resonances from short periodic orbits, *Phys. Rev. E* **80**, 035202(R) (2009).
- [65] G. G. Carlo, R. M. Benito, and F. Borondo, Theory of short periodic orbits for partially open quantum maps, *Phys. Rev. E* **94**, 012222 (2016).
- [66] M. Degli Esposti and S. Graffi, Mathematical aspects of quantum maps, in [80], pp. 49–90.
- [67] Y. V. Fyodorov and H.-J. Sommers, Statistics of resonance poles, phase shifts and time delays in quantum chaotic scattering: Random matrix approach for systems with broken time-reversal invariance, *J. Math. Phys.* **38**, 1918 (1997).
- [68] H. Schomerus, From scattering theory to complex wave dynamics in non-hermitian \mathcal{PT} -symmetric resonators, *Phil. Trans. R. Soc. A* **371**, 20120194 (2013).
- [69] K. Husimi, Some formal properties of the density matrix, *Proc. Phys. Math. Soc. Jpn.* **22**, 264 (1940).
- [70] Y. V. Fyodorov and H.-J. Sommers, Spectra of random contractions and scattering theory for discrete-time systems, *J. Exp. Theor. Phys. Lett.* **72**, 422 (2000).
- [71] K. Życzkowski and H.-J. Sommers, Truncations of random unitary matrices, *J. Phys. A* **33**, 2045 (2000).
- [72] H. Schanz, Phase-space correlations of chaotic eigenstates, *Phys. Rev. Lett.* **94**, 134101 (2005).
- [73] B. V. Chirikov, A universal instability of many-dimensional oscillator systems, *Phys. Rep.* **52**, 263 (1979).
- [74] M. V. Berry, N. L. Balazs, M. Tabor, and A. Voros, Quantum maps, *Ann. Phys. (N.Y.)* **122**, 26 (1979).
- [75] S.-J. Chang and K.-J. Shi, Evolution and exact eigenstates of a resonant quantum system, *Phys. Rev. A* **34**, 7 (1986).
- [76] V. I. Arnold and A. Avez, *Ergodic Problems of Classical Mechanics* (Benjamin, New York, 1968).
- [77] N. L. Balazs and A. Voros, The quantized baker’s transformation, *Ann. Phys.* **190**, 1 (1989).
- [78] M. Saraceno, Classical structures in the quantized baker transformation, *Ann. Phys. (N.Y.)* **199**, 37 (1990).
- [79] R. G. Gallager, *Circularly-symmetric Gaussian random vectors* (2008), preprint.
- [80] M. Degli Esposti and S. Graffi, eds., *The Mathematical Aspects of Quantum Maps*, *Lect. Notes Phys.*, Vol. 618 (Springer-Verlag, Berlin, 2003).